Personnalized Spinal Cord Reconstruction using Machine Learning

EPFL CS-433 Machine Learning Project 2 — **Team TheOutliers2**
Leon Muller (*leon.muller@epfl.ch*), Anasse El Boudiri (*anasse.elboudiri@epfl.ch*), Jan Steiner (*jan.steiner@epfl.ch*)
In collaboration with the **EPFL .NeuroRestore Lab** (https://www.neurorestore.swiss/)
Supervised by **Prof. Grégoire Courtine** and **Sergio Daniel Hernandez Charpak**
https://github.com/CS-433/ml-project-2-theoutliers2

***Abstract*—Spinal cord injuries (SCI) often result in severe paralysis and loss of motor functions, requiring accurate, patient-specific 3D spinal cord models for advanced neuroprosthetic interventions. Manual segmentation of these models is time-intensive, motivating the use of machine learning to automate this process. This study focuses on segmenting thin, closely packed spinal roots using a dataset of 41 MRI scans. We worked with two architectures: nnU-Net, known for its adaptability, and HarDNet, a lightweight and efficient backbone. To address data limitations, we developed an automated pre-processing and augmentation pipeline to improve consistency and balance. Our results demonstrate the feasibility of automating spinal cord segmentation and show the practical utility of the models in generating pre-annotations. nnU-Net achieves strong results and HarDNet shows potential for future optimization. This work lays the groundwork for personalized spinal cord reconstruction and innovative neuroprosthetic solutions for SCI patients.**

I. Introduction

Spinal Cord Injury (SCI) is a major global health issue, with 0.9 million new cases and 20.6 million people living with SCI reported in 2019 [1]. These injuries often result in severe paralysis and long-term disabilities due to damage to the spinal cord, which connects the brain and the body. This disruption leads to the loss of motor functions like walking and standing, as well as sensory and autonomic functions.

The EPFL .NeuroRestore Lab is pioneering innovative neuroprosthetic solutions to help SCI patients regain lost motor functions. Their approach involves implanting Electrocorticography (ECoG) arrays on the brain [2] and electrodes on the spinal cord for Epidural Electrical Stimulation (EES)[2], [3], [4], [5], [6]. Using deep learning algorithms to process brain signals, their devices deliver EES to the region below the injury in the lumbar [4], [2], [3], [5] or lower thoracic [6] regions, restoring communication and enabling movement.

As these interventions are invasive, highly detailed and patient-specific 3D models of the spinal cord are essential for surgical planning and ensuring the safety of these procedures[3]. However, current spinal cord segmentation from MRI data is done manually[3], which is time-consuming and prone to variability. Automating this process could greatly improve efficiency, consistency, and precision, benefiting both clinicians and patients.

This project aims on using machine learning to automate the segmentation of spinal cord structures, with a specific focus on spinal roots. These roots play a vital role in transmitting signals between the spinal cord and peripheral nerves and contain the structures first activated by EES[3]. They present significant challenges for segmentation due to their small diameter (0.2-0.3 mm) and the presence of surrounding tissue noise in MRI images.

Existing methods for segmentation in other areas, like the cervical region[7] or animal models such as felines [8], have shown promising results. However, the human lower thoracic and lumbosacral spinal cord is more complex. The spinal roots are closely packed together, with roots from several spinal levels visible on the same axial level (Figure 7). To tackle this, we will compare two approaches: the nnU-Net framework [9], [10], which has shown promise on the cervical region [7], and the HarDNet lightweight backbone [11] [12], which has been effective in feline models[8]. Our goal is to improve these methods by adding better data pre-processing and post-processing steps, helping the models work faster and produce more accurate results for this challenging task.

II. Models and Methods

A. Data Exploration

The dataset, provided by the EPFL .NeuroRestore Lab, consists of 41 3D T2 MRI scans of the spinal cord, covering a wide range of anatomical variations from the T6 vertebra to S3. These high-resolution scans, stored in NIfTI format, include manually annotated segmentation masks for fat, cerebrospinal fluid (CSF), white matter (WM), and spinal roots. Figure 5 illustrates the spinal cord anatomy and its components.

The dataset presents several challenges. With only 41 scans available, it offers a limited sample size for a task as complex as 3D segmentation. Furthermore, not all scans are fully annotated. The labels are highly unbalanced, with some classes having only one or two images available. Additionally, the high detail in the MRI scans can introduce artefacts, losses in signal, which affect image quality. The segmentation of thin spinal roots is particularly challenging

due to their small size, proximity to one another, and the surrounding tissue noise. These factors emphasize the importance of robust data pre-processing and augmentation strategies to enhance the dataset and improve model performance.

The primary objective of this project is to segment the spinal roots, which are by far the most difficult structures to identify. As such, the focus was placed on extracting and analyzing segmentation masks specifically for these spinal roots.

For each MRI scan, three types of masks are provided:

- **Spinal Roots as One Entity**: A single mask that combines all spinal roots.
- **Spinal Roots by Vertebrae Level**: Masks that group spinal roots by vertebrae level (e.g., T6, T7, T8, etc.).
- **Spinal Roots Individually Segmented**: Individual masks that separate each spinal root by side (left or right), type (ventral or dorsal), and vertebrae level.

Figure 1 displays a vertical slice of an MRI scan with segmented dorsal spinal roots, while Figure 6 provides a 3D rendering of segmented dorsal spinal roots.

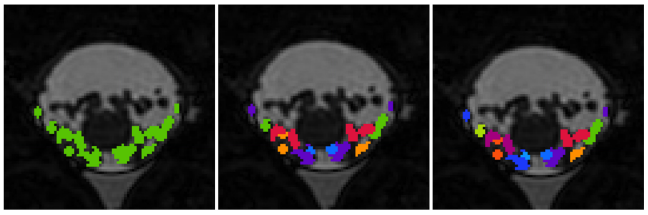

1. One-entity mask 2. Grouped by vertebrae level mask 3. Individually segmented mask

Figure 1. Example of an axial slice of a spinal cord MRI image with the dorsal spinal roots segmented grouped as (1) one entity, (2) per spinal level and (3) per individual roots.

B. Data Pre-processing

Pre-processing was a critical step in refining the dataset. One of the key issues identified was the underrepresentation of certain regions, such as cervical, upper thoracic, and lower sacral roots, as well as the sparse annotation of ventral roots compared to dorsal roots. To address these disparities, we concentrated on the lower thoracic, lumbar, and upper sacral dorsal roots, which are most relevant for electrode implantation procedures. This refinement reduced the number of segmentation classes from 120 to 22, simplifying the task and improving focus.

To improve the quality of segmentation masks, we used the more reliable spinal roots-as-one-entity masks to refine the individual spinal root masks. We noticed inconsistencies in the individual annotations, so we created a custom flood-fill algorithm. This algorithm expands segmentation classes from the initial masks to neighboring voxels, aligning them with the one-entity masks. This approach significantly enhanced the consistency and quality of the individual segmentations.

Finally, all MRI images and segmentations were cropped to focus only on regions with annotations. This removed irrelevant parts, like unsegmented spinal roots, and reduced image size. By isolating key areas, this step provided cleaner training data and reduced computational load.

All these pre-processing steps are part of an automated pipeline, now available for the lab to preprocess datasets quickly and consistently. This saves time and reduces variability compared to manual processing.

C. Data Augmentation

To address the dataset's imbalance and limited size, we implemented a data augmentation pipeline to improve model robustness and reduce overfitting. The augmentations preserved the anatomical integrity of the MRI images while increasing training sample diversity through transformations like rotation, translation, scaling, blurring, and gamma correction, applied randomly within set limits.

We focused on addressing class imbalance by prioritizing underrepresented regions, such as mid-thoracic roots. Targeted augmentation increased the samples for these classes, improving balance and ensuring the model was exposed to less frequent structures. Figure 2 illustrates the distribution of segmentation labels in the dataset before and after pre-processing and augmentation.

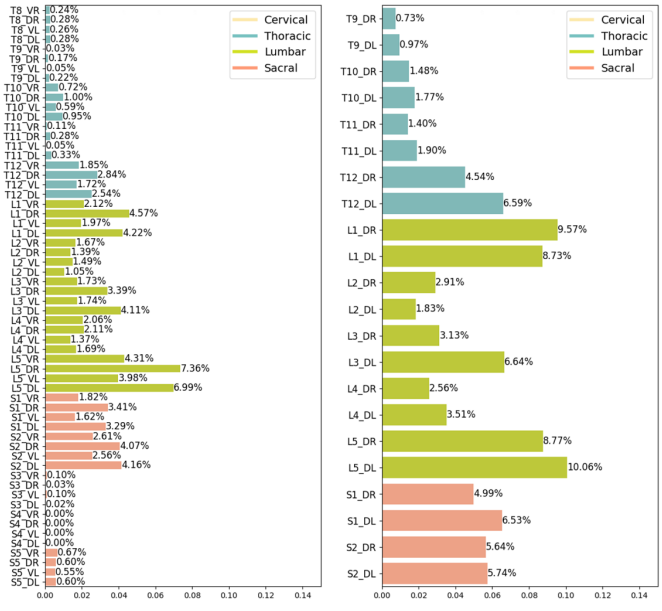

1. Distribution before augmentation 2. Distribution after augmentation

Figure 2. Distribution of different types of segmentations in the dataset, following the format: {Region (T6, T7, T8, etc.)}_{Type (D for Dorsal, V for Ventral)}{Side (L for Left, R for Right)}.

This pipeline expanded the dataset, improved diversity, addressed class imbalances, and enhanced the model's ability to generalize. Combined with pre-processing, it offers an efficient workflow for preparing data for training.

D. Machine Learning Models

Due to the uniqueness of this task, no existing baselines are directly applicable, requiring us to establish our own baseline for this highly complex problem. We drew inspiration from architectures that have succeeded in similar but less complex problems. For example, Valosek and colleagues [7] achieved a Dice Score of 0.658 for cervical spine segmentation using nnU-Net, a simpler task since only one spinal root is present at each spinal level as shown by Figure 7. Similarly, another study [8] reported a binary Dice Score of 0.73 for 2D segmentation of feline spinal cords using a modified HarDNet backbone. Unlike humans, feline spinal roots are larger (2-5 mm vs. 0.2-3 mm) and more visible. Additionally, that study used three input channels (T2-weighted, fat-enhanced, and 19F images), while we only had T2 images, increasing the complexity of our task.

Building on these insights, we first worked with nnU-Net, a state-of-the-art deep learning framework for medical image segmentation[9]. nnU-Net dynamically adapts its configuration to the characteristics of specific datasets, leveraging its U-Net encoder-decoder architecture to handle diverse medical segmentation tasks effectively. This flexibility made nnU-Net a robust starting point for our work.

We also implemented HarDNet, a lightweight and efficient backbone designed for 2D image segmentation [11]. HarDNet's potential for 3D segmentation was demonstrated in the feline spinal cord study, which detailed architectural modifications to be efficient on 3D multi-class segmentation [8]. Based on this work, we implemented similar but also dataset tailored modifications, consulting with the study's authors to ensure accurate adaptation. Figure 8 illustrates the modified architecture implemented in our project, alongside an example of the model's input and output. We adapted the 3D MRI data to make it compatible with the architecture by extracting a square region around the spinal cord centerline for each vertica slice. The centerline was detected using the Spinal Cord Toolbox (SCT) [13]. If the region extended beyond the image boundaries, padding was applied to ensure completeness. This approach ensured the centerline remained at the center while preserving all the critical information needed for spinal root detection.

III. Results

A. Models' Performance

Building on the machine learning models discussed earlier, we evaluated their performance through a training and testing process. The primary focus was on nnU-Net, which was trained for 500 epochs (about 16 hours) on the .NeuroRestore infrastructure. The model utilized a combined loss function of Dice (targeting segmentation shapes) and Cross-Entropy (focusing on class distribution), was trained on the 3D full resolution images, and the training configuration used was nnUNetResEncUNetMPlans which sets up all the hyperparameters for the training.

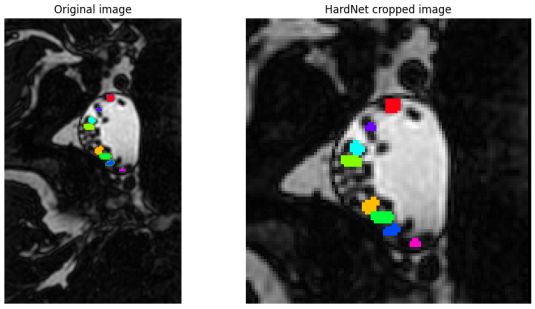

Figure 3. Comparison before and after HardNet personalized image preprocessing.

Initially, training aimed to segment preprocessed individual spinal roots across all regions. However, since the model faced difficulties, we introduced data augmentation and adjusted our approach. Instead of segmenting all roots at once, we segmented the spinal cord by spinal level and applied post-processing to distinguish left and right roots at each level, generating individual segmentation masks. This post-processing utilized the SCT to extract the spinal cord's centerline and separate the roots.

Recognizing the variability in anatomical characteristics across different spinal regions, we divided the model into multiple models, each focusing on a specific region (thoracic, lumbar, sacral). This approach allowed us to concentrate on distinct regions with unique characteristics.

The models were evaluated using the binary Dice score, a widely used metric for segmentation quality [14]. While labels were not the primary concern, as they could be easily adjusted by annotators, the model still needed to correctly differentiate individual roots. This requirement led us to measure an expert score, providing insights into the usefulness of the segmentations. The objective was to generate pre-annotations that minimized manual effort. Practical utility was further assessed through expert evaluations. An expert score of 0.5 indicates no added value from the model, while a score of 1.0 signifies a complete reduction in the expert's workload. Table I summarizes the model's performance, and Figure 4 shows a visual example of the model's prediction.

As expected, data augmentation enhanced the model's generalization capabilities, and models trained on spinal levels with post-processing outperformed those focused on individual roots. However, contrary to expectations, the region-specific models did not surpass the all-spinal model. After examining the data, we found that in some images, roots from adjacent regions were visible, leading the model to attempt segmentation beyond the intended target area.

Region - Model	Binary Dice Score	Expert Score
All - Invididuals (Non-augmented)	0.278 ± 0.187	—
All - Invididuals	0.293 ± 0.173	—
All - Spinal levels	**0.311 ± 0.165**	0.78 ± 0.04
Sacral - Spinal levels	0.259 ± 0.135	**0.85 ± 0.00**
Lumbar - Spinal levels	0.241 ± 0.164	0.73 ± 0.11
Thoracic - Spinal levels	0.220 ± 0.182	—

Table I
NNUNET MODELS' PERFORMANCE COMPARISON.

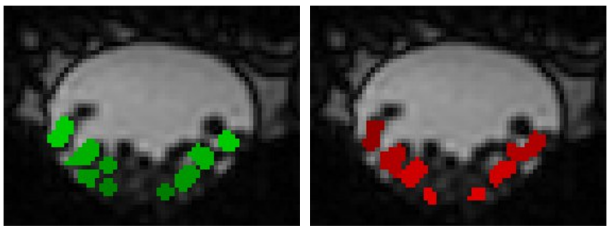

1. Ground Truth 2. Model's Prediction

Figure 4. Example of an axial slice of a spinal cord high resolution MRI image. Manually label dorsal roots are visible in green (1. Ground Truth). Our model's predicted dorsal roots are visible in red (2. Model's prediction).

This overlap likely contributed to the reduced performance of region-specific models. Notably, this issue is absent in the cervical region, where each level contains only one root, as visible in Figure 7, motivating our decision to focus on specific regions.

The expert scores provide a practical perspective, underlying the utility of our results. These underscore the usefulness of the models in generating pre-annotations that reduce manual effort, reinforcing their potential clinical value.

We implemented and tested HarDNet, which showed promise by overfitting on a small subset of 2D images. However, due to time constraints, we couldn't optimize it, resulting in long training times and preventing full-dataset training. With further refinement and resources, HarDNet could achieve strong results for this challenging task.

IV. FURTHER DISCUSSION

Several aspects could be further explored.

One of the primary limitations of this project was the dataset. With only 41 scans, the size is small for this complex task even if it is the largest annotated dataset in the field. Furthermore, the annotations are imbalanced, as certain classes, such as ventral roots and upper thoracic regions, are underrepresented. Addressing these limitations could involve creating additional annotated datasets or using synthetic data generation to augment the dataset further.

Improving annotation quality is another critical aspect. Collaborative annotation could be employed to leverage the expertise of multiple annotators, ensuring consistent and accurate annotations. However, this approach requires additional resources and time, making it less feasible.

To simplify the complex task and improve performance, a two-stage modeling approach could be used. First, a binary segmentation model would detect spinal roots as a single entity. Its output would then feed into a second model that classifies each pixel into specific spinal root classes based on side, type, and vertebrae level. This approach reduces the challenge of directly segmenting individual roots by letting the classification model focus only on pixels already identified as spinal roots.

Finally, the HarDNet architecture shows promise for this task, but further optimization is needed to provide results. Speed up and memory optimization techniques could be used to make the full-dataset training feasible.

V. CONCLUSION

This project showcases the feasibility of using machine learning to segment spinal cord roots and establishes a first baseline for the thoracic, lumbar, and sacral regions, addressing the challenges of segmenting thin and closely packed spinal roots.

The nnU-Net performed well, benefiting from data augmentation and post-processing, we achieved a binary dice score of **0.311 ± 0.164** on the all-spinal levels model. The model's expert score ranges between **0.73 and 0.85**, indicating its practical utility in generating pre-annotations. HarDNet showed promise by overfitting on a subset of the data and is worth exploring for future improvements. However, the small dataset size and class imbalance constrained the models' ability to generalize, underscoring the need for larger, better-annotated datasets.

This work lays the foundation for personalized spinal cord reconstruction, crucial for advanced neuroprosthetic solutions. Future efforts should prioritize expanding the dataset, refining HarDNet, and optimizing models for efficiency. By integrating machine learning with domain expertise, this study takes a step toward improving spinal cord injury treatment and advancing neuroprosthetic technology.

Model	FP Precision	Size (MB)	Inference Time (s)	Binary Dice Score
nnU-Net	32-bit	1459.67	147	0.311 ± 0.164
nnU-Net	16-bit	729.83	96	0.293 ± 0.176

Table II
MODEL'S SIZE AND DICE SCORE BEFORE AND AFTER THE QUANTIZATION PROCESS

A. Ethical Assessment

The segmentation method employed relies on nnU-Net, a highly complex architecture with a significant number of parameters. While effective, this approach is computationally intensive, requiring days of training, substantial GPU memory, and power. This raises concerns about ecological sustainability and the environmental impact of such resource-heavy methods. To address this, we explored the HarDNet backbone, a lightweight alternative that requires less GPU memory, power, and training time, thereby reducing the carbon footprint of the model[11].

Additionally, we implemented a post-training quantization (PTQ) process, as demonstrated in previous studies [15], to optimize model inference time and memory usage. This process involves downgrading the floating-point precision (e.g., from 32-bit to 16-bit) of the model weights after training to reduce the model's size and inference time. However, quantization also reduces the model's performance, necessitating a balance between model size and metrics scores. Table II compares the model's size, inference time, and binary dice score before and after the quantization process.

Beyond environmental considerations, the ethical implications of such trade-off methods must be discussed, as the models directly impact patient care and outcomes. A less accurate model could introduce errors in the segmentation process, leading to incorrect surgical planning and potential harm to patients. Therefore, it is essential to balance the model's efficiency and performance to ensure patient safety and the quality of care. Partially accurate results can assist experts in manual segmentation, reducing the time required for surgical planning and potentially laying the groundwork for scaling up EES therapies.

REFERENCES

[1] W. Ding, S. Hu, P. Wang, H. Kang, R. Peng, and Y. Dong, "Spinal cord injury: The global incidence, prevalence, and disability from the global burden of disease study 2019," *Spine*, vol. Publish Ahead of Print, 07 2022.

[2] H. Lorach, A. Galvez, V. Spagnolo, F. Martel, S. Karakas, N. Intering, M. Vat, O. Faivre, C. Harte, S. Komi, J. Ravier, T. Collin, L. Coquoz, I. Sakr, E. Baaklini, S. D. Hernandez-Charpak, G. Dumont, R. Buschman, N. Buse, T. Denison, I. Van Nes, L. Asboth, A. Watrin, L. Struber, F. Sauter-Starace, L. Langar, V. Auboiroux, S. Carda, S. Chabardes, T. Aksenova, R. Demesmaeker, G. Charvet, J. Bloch, and G. Courtine, "Walking naturally after spinal cord injury using a brain–spine interface," *Nature*, vol. 618, no. 7963, pp. 126–133, Jun. 2023. [Online]. Available: https://www.nature.com/articles/s41586-023-06094-5

[3] A. Rowald, S. Komi, R. Demesmaeker, E. Baaklini, S. D. Hernandez-Charpak, E. Paoles, H. Montanaro, A. Cassara, F. Becce, B. Lloyd, T. Newton, J. Ravier, N. Kinany, M. D'Ercole, A. Paley, N. Hankov, C. Varescon, L. McCracken, M. Vat, M. Caban, A. Watrin, C. Jacquet, L. Bole-Feysot, C. Harte, H. Lorach, A. Galvez, M. Tschopp, N. Herrmann, M. Wacker, L. Geernaert, I. Fodor, V. Radevich, K. Van Den Keybus, G. Eberle, E. Pralong, M. Roulet, J.-B. Ledoux, E. Fornari, S. Mandija, L. Mattera, R. Martuzzi, B. Nazarian, S. Benkler, S. Callegari, N. Greiner, B. Fuhrer, M. Froeling, N. Buse, T. Denison, R. Buschman, C. Wende, D. Ganty, J. Bakker, V. Delattre, H. Lambert, K. Minassian, C. A. T. van den Berg, A. Kavounoudias, S. Micera, D. Van De Ville, Q. Barraud, E. Kurt, N. Kuster, E. Neufeld, M. Capogrosso, L. Asboth, F. B. Wagner, J. Bloch, and G. Courtine, "Activity-dependent spinal cord neuromodulation rapidly restores trunk and leg motor functions after complete paralysis," *Nature Medicine*, vol. 28, no. 2, pp. 260–271, Feb. 2022. [Online]. Available: https://www.nature.com/articles/s41591-021-01663-5

[4] F. B. Wagner, J.-B. Mignardot, C. G. Le Goff-Mignardot, R. Demesmaeker, S. Komi, M. Capogrosso, A. Rowald, I. Seáñez, M. Caban, E. Pirondini, M. Vat, L. A. McCracken, R. Heimgartner, I. Fodor, A. Watrin, P. Seguin, E. Paoles, K. Van Den Keybus, G. Eberle, B. Schurch, E. Pralong, F. Becce, J. Prior, N. Buse, R. Buschman, E. Neufeld, N. Kuster, S. Carda, J. von Zitzewitz, V. Delattre, T. Denison, H. Lambert, K. Minassian, J. Bloch, and G. Courtine, "Targeted neurotechnology restores walking in humans with spinal cord injury," *Nature*, vol. 563, no. 7729, pp. 65–71, Nov. 2018. [Online]. Available: http://www.nature.com/articles/s41586-018-0649-2

[5] C. Kathe, M. A. Skinnider, T. H. Hutson, N. Regazzi, M. Gautier, R. Demesmaeker, S. Komi, S. Ceto, N. D. James, N. Cho, L. Baud, K. Galan, K. J. E. Matson, A. Rowald, K. Kim, R. Wang, K. Minassian, J. O. Prior,

L. Asboth, Q. Barraud, S. P. Lacour, A. J. Levine, F. Wagner, J. Bloch, J. W. Squair, and G. Courtine, "The neurons that restore walking after paralysis," *Nature*, vol. 611, no. 7936, pp. 540–547, Nov. 2022. [Online]. Available: https://www.nature.com/articles/s41586-022-05385-7

[6] J. W. Squair, M. Gautier, L. Mahe, J. E. Soriano, A. Rowald, A. Bichat, N. Cho, M. A. Anderson, N. D. James, J. Gandar, A. V. Incognito, G. Schiavone, Z. K. Sarafis, A. Laskaratos, K. Bartholdi, R. Demesmaeker, S. Komi, C. Moerman, B. Vaseghi, B. Scott, R. Rosentreter, C. Kathe, J. Ravier, L. McCracken, X. Kang, N. Vachicouras, F. Fallegger, I. Jelescu, Y. Cheng, Q. Li, R. Buschman, N. Buse, T. Denison, S. Dukelow, R. Charbonneau, I. Rigby, S. K. Boyd, P. J. Millar, E. M. Moraud, M. Capogrosso, F. B. Wagner, Q. Barraud, E. Bezard, S. P. Lacour, J. Bloch, G. Courtine, and A. A. Phillips, "Neuroprosthetic baroreflex controls haemodynamics after spinal cord injury," *Nature*, vol. 590, no. 7845, pp. 308–314, Feb. 2021. [Online]. Available: http://www.nature.com/articles/s41586-020-03180-w

[7] J. Valošek, T. Mathieu, R. Schlienger, O. S. Kowalczyk, and J. Cohen-Adad, "Automatic segmentation of the spinal cord nerve rootlets," *Imaging Neuroscience*, vol. 2, p. 1–14, 2024. [Online]. Available: http://dx.doi.org/10.1162/imag_a_00218

[8] A. Fasse, T. Newton, L. Liang, U. Agbor, C. Rowland, N. Kuster, R. Gaunt, E. Pirondini, and E. Neufeld, "A novel cnn-based image segmentation pipeline for individualized feline spinal cord stimulation modeling," *Journal of Neural Engineering*, vol. 21, no. 3, p. 036032, jun 2024. [Online]. Available: https://dx.doi.org/10.1088/1741-2552/ad4e6b

[9] F. Isensee, P. F. Jaeger, S. A. A. Kohl, J. Petersen, and K. H. Maier-Hein, "nnU-Net: a self-configuring method for deep learning-based biomedical image segmentation," *Nature Methods*, vol. 18, no. 2, pp. 203–211, 2021, _eprint: 1904.08128.

[10] F. Isensee, T. Wald, C. Ulrich, M. Baumgartner, S. Roy, K. Maier-Hein, and P. F. Jaeger, "nnu-net revisited: A call for rigorous validation in 3d medical image segmentation," 2024. [Online]. Available: https://arxiv.org/abs/2404.09556

[11] C.-H. Huang, H.-Y. Wu, and Y.-L. Lin, "Hardnet-mseg: A simple encoder-decoder polyp segmentation neural network that achieves over 0.9 mean dice and 86 fps," 2021. [Online]. Available: https://arxiv.org/abs/2101.07172

[12] P. Chao, C.-Y. Kao, Y.-S. Ruan, C.-H. Huang, and Y.-L. Lin, "Hardnet: A low memory traffic network," 2019. [Online]. Available: https://arxiv.org/abs/1909.00948

[13] B. D. Leener, S. Lévy, S. M. Dupont, V. S. Fonov, N. Stikov, D. L. Collins, V. Callot, and J. Cohen-Adad, "Sct: Spinal cord toolbox, an open-source software for processing spinal cord {MRI} data," *NeuroImage*, vol. 145, Part A, pp. 24 – 43, 2017. [Online]. Available: https://www.sciencedirect.com/science/article/pii/S1053811916305560

[14] D. Müller, I. Soto-Rey, and F. Kramer, "Towards a guideline for evaluation metrics in medical image segmentation," 2022. [Online]. Available: https://arxiv.org/abs/2202.05273

[15] M. Nagel, M. Fournarakis, R. A. Amjad, Y. Bondarenko, M. van Baalen, and T. Blankevoort, "A white paper on neural network quantization," 2021. [Online]. Available: https://arxiv.org/abs/2106.08295

[16] S. . P. C. of North America, "Official website," https://www.sapnamed.com.

[17] OpenAI, "Chatgpt," https://chatgpt.com/, 2024.

APPENDIX

A. *Figures*

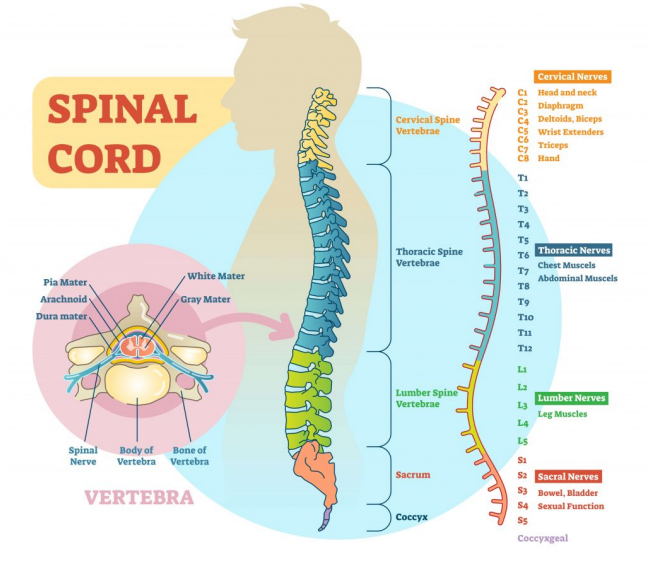

Figure 5. Neuro-anatomy of the spinal cord. (Left panel) Axial cut of the spinal cord tissues. (Center panel) Vertebrae levels of the spine, divided into cervical, thoracic, lumbar and the sacrum. (Right panel) Spinal levels, defined as the merging regions of spinal nerves with the spinal cord, dimensions differ from individual to individual as well as their relative location with respect to the vertebrae. Source: Spine & Pain Clinics of North America [16]

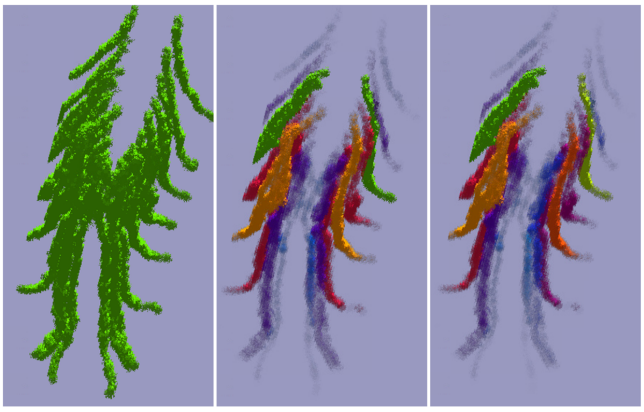

1. One-entity mask | 2. Grouped by vertebrae level mask | 3. Individually segmented mask

Figure 6. 3-dimensional visualization of dorsal roots of the lumbo-sacral region grouped as (1) one entity, (2) per spinal level and (3) per individual roots.

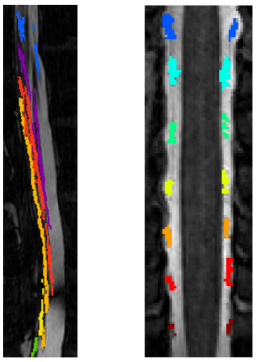

1. Lumbar segmentations | 2. Cervical Segmentations

Figure 7. Sagittal view and coronal view of spinal roots segmentation in the (1) lumbo-sacral and (2) cervical regions respectively. Different colors represent spinal roots from different spinal levels. Several roots are overlapping on the lumbo-sacral region whereas the cervical roots are visibly separated. Cervical roots were segmented by Valosek et al. (2024)[7].

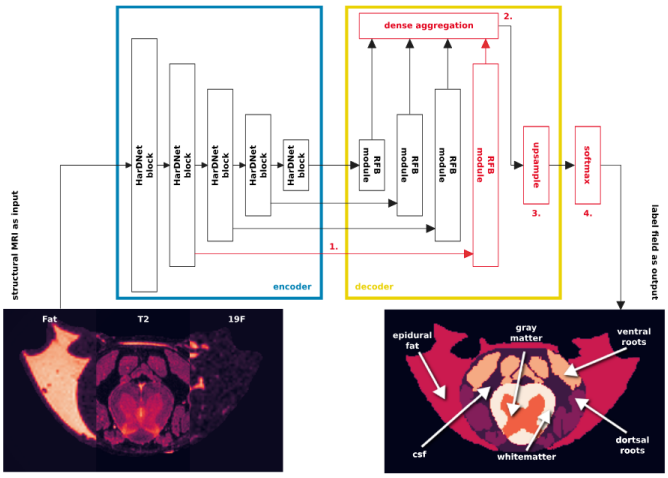

Figure 8. HarDNet architecture for feline spinal cord segmentation described by Fasse et al. (2024)[8] alongside an example of the model's input and output. Source: A novel CNN-based image segmentation pipeline for individualized feline spinal cord stimulation modeling

B. *AI usage*

ChatGPT [17] was used to rephrase the whole report, to keep consistency and coherence in the writing style.